Progress In Electromagnetics Research M, Vol. 86, 183–192, 2019

Study of Transmitter Interference to Receiver at 2 GHz with High Antenna Port Isolation

Marko Sonkki[1, *], Janne Aikio[2], Marko E. Leinonen[1], and Aarno Pärssinen[1]

Abstract—The paper presents simulated and measurement results of a planar antenna structure at 2 GHz center frequency. The antenna has two ports implemented into the same conductive body. The antenna shows measured −10 dB impedance bandwidth from 1.87 GHz to 2.18 GHz with average 41.3 dB isolation between the antenna ports over the studied frequency bandwidth. Antenna is used to measure transmitted WCDMA FDD signal leakage to the receiver with a presence of blocker signal, which is transmitted over the air. The system measurements show that the RF filtering requirements can be relaxed based on 3GPP standard by using highly isolated antenna structure. Application areas can be found at both ends of the mobile communications system, mobile devices, and small cell base stations.

1. INTRODUCTION

In wireless communications, a need to reduce bulky and costly RF (radio frequency) filtering has been evident, but it is an extremely challenging problem since the birth of commercial mass market. The problem gets even worse in the case of 3GPP (The 3rd Generation Partnership Project) new standard release for long term evolution (LTE), where 63 bands have been standardized and out of them, frequency division duplexing (FDD) multiplexing has been standardized for 43 bands [1]. Moreover, the LTE standard specifies 640 inter-band carrier aggregation combinations, which need to be taken into account in filter designs of mobile devices. Low cost with low power and spectral efficient communication modes are needed to achieve the demanding goals for both long range and local monitoring applications.

The main challenge for designing FDD and full duplex (FD) networks is the massive self-interference caused by the own transmission (TX) interference on the signal reception (RX). The transmission may interfere the reception by blocking the reception signal due to limited linearity of the receiver, or the transmission generates a wideband noise over the received signal. The operation frequencies vary with different radio applications, but the basic paradigm is the same: How to provide sufficient isolation between TX and RX ports in the case of a complex communications network?

FDD is the mainstream technology in cellular networks including Wideband Code Division Multiple Access/High Speed Packet Access (WCDMA/HSPA) for 3G (Third Generation Mobile Networks), and LTE for 4G (Fourth Generation Mobile Networks). In both cases, several frequency bands are needed to cover the needs of end-users globally. A high-end commercial mobile device (phone or other) can support nearly 30 frequency bands today [2], and the demands increase when heading towards 5G (Fifth Generation Mobile Networks).

Each frequency band requires a dedicated duplex filter to isolate TX signals from RX port in the FDD RF front-end. This adds significant amount of complexity and cost in modern mobile devices and small cell base stations. In small cell base stations, the environment can be seen more stable than

Received 1 August 2019, Accepted 15 November 2019, Scheduled 26 November 2019

* Corresponding author: Marko Sonkki (marko.sonkki@gmail.com).

[1] Centre for Wireless Communications (CWC), University of Oulu, P. O. B. 4500, FIN-90014, Finland. [2] Circuit and Systems Research Unit, University of Oulu, P. O. B. 4500, FIN-90014, Finland.

mobile stations. If one can provide an antenna with significant isolation between RX and TX ports, the requirements of the subsequent signal processing elements, like RF-filters, could be relaxed.

An antenna isolation in the order of 30–40 dB will not completely remove the need for RF-filtering but make it a lot easier. Potentially more flexible filtering could be implemented, and the cost and component count and/or complexity can be reduced. A tunable RF front-end (RFFE) has been proposed in [3] to improve the linearity of the RF front-end by including an adaptive RF canceller with fixed surface acoustic wave (SAW) filters.

In extreme case of FDD, the frequency spacing between RX and TX is zero, i.e., receiver and transmitter are operating at the same time at the same channel. The technique is called in-band full duplex [4]. It promises massive improvements in channel capacity by ushering in a paradigm shift in the design of existing networking protocols. Before its inception, time division duplex (TDD) communication was the de-facto standard, i.e., nodes may either transmit or receive at any given time when the same band/channel was used both for uplink and downlink, like in LTE TDD mode [1]. This key assumption influenced the design of the protocol stack, especially the channel access mechanism at the link layer. As a result, any simultaneous use of the channel by more than one node within their interference range in the same network could cause the transmitted packets to collide. This, in turn, resulted in the waste of bandwidth resources and required retransmission by every contending nodes that suffered packet losses. With the advent of the FD-technology, this problem of simultaneous channel access can be theoretically mitigated to a large extent, and the existing spectrum can be utilized to far greater extent.

Achieving a sufficient isolation between TX and RX is a major research challenge. This will be done in phases, i.e., sufficient RF or analog isolation/cancellation is required to avoid any compression in the receiver analog signal processing and to avoid excessive amount of additional bits in analog-digital converter (ADC). After that, the digital signal processing is needed to do the rest. Any additional RF-isolation that can be provided will relax design and signal processing requirements. Thus, any antenna structure that provides good isolation between two antenna ports (TX and RX) significantly helps system design and specifications of other blocks.

Compared to the recently published papers [5–26], it can be seen how 40 dB or better antenna port isolation is difficult to achieve without decoupling network or structure. This work presents measurement results of a novel planar two-port antenna structure around 2 GHz with average 41.3 dB isolation between the TX and RX ports in an FDD system. The study is done by measuring the TX signal leakage level to the RX and varying interfering signal level to quantify the level of the Intermodulation Distortion (IMD).

The paper is organized as follows. Section 2 presents the studied antenna structure with radiation properties at 2 GHz and S-parameter performance. In Section 3, the 3GPP transceiver filtering requirements are explained. Section 4 shows the RF measurement setup and measured results. Finally, Section 5 concludes the results.

2. ANTENNA OPERATING MECHANISM AND ANTENNA STRUCTURE WITH SIMULATED AND MEASURED RESULTS

This section presents the operating mechanism of the proposed antenna structure studied in this paper with the dimensions, simulated radiation properties at 2 GHz, and simulated and measured S-parameters as a function of frequency. CST MWS (Computer Simulation Technology Microwave Studio) with Finite-Difference Time-Domain (FDTD) method is used in antenna simulations (see Fig. 1(d), Fig. 2(c) and Fig. 4). Keysight PNA-X is used in the conductive S-parameter measurements.

2.1. Antenna Operating Mechanism

The principal of the proposed antenna operating mechanism is presented in Figs. 1(a)–(c). The feeds are designed so that two orthogonal radiating modes, Mode 1 (Fig. 1(a)) and Mode 2 (Fig. 1(b)), can be excited on a common conducting body (Fig. 1(c)) with high antenna port isolation. Mode 1 can be seen as a fundamental mode whereas Mode 2 is a higher order mode. In other words, where Mode 1 has a maximum, marked at the point of the dotted line, Mode 2 has a minimum. Fig. 1(d) presents the simulated surface current distributions where Port 1 and Port 2 (ports shown in Fig. 2(a)) are excited

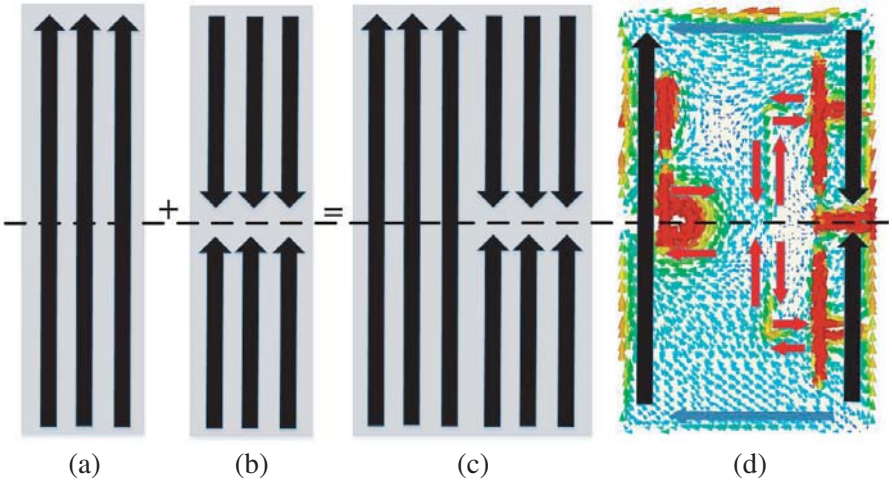

Figure 1. Antenna operating mechanism. (a) A principal of surface currents of Mode 1 excited with Port 1. (b) A principal of surface currents of Mode 2 excited with Port 2. (c) A principal of combined surface currents of Mode 1 and Mode 2 in a common conducting body. (d) Simulated surface current distributions of Port 1 and Port 2 (ports shown in Fig. 2(a)) excited simultaneously with same amplitude and equal phase at 2 GHz.

simultaneously with the same amplitude and equal phase. In Fig 1(d), the horizontal currents represent (arrows with blue color) a wakening higher order mode.

The surface currents around the slots propagate in opposite directions (arrows with red color) and, thus, are cancelled in the far-field. As one can notice, the surface currents in Fig. 1(d) well correspond to the principal modes in Figs. 1(a) and (b): Mode 1 has a maximum aligned of the dotted line, where Mode 2 has a minimum.

2.2. Antenna Structure with Simulated Radiation Properties

Figure 2(a) presents the studied planar antenna structure with a coordinate system and dimensions in millimeters. Port 1 is positioned in the upper left corner, and Port 2 appears in the right middle. The antenna is fabricated on Rogers 4003C RF-laminate with 0.813 mm substrate thickness, in which one side is the antenna structure, and the other side is the feedlines of Port 1 and Port 2. Port 1 is fed with an SMA (SubMiniature version A) coaxial probe, whereas Port 2 is fed with an SMA edge connector, as can be seen in Fig. 3, which shows pictures of the prototype antenna. Fig. 2(b) presents the side view of the antenna structure aligned with the line of dots and dashes (Y-Y cut). The side view is up scaled to better illustrate the small differences in the structure as PCB copper thickness is 35 µm. Notice that the prototype antenna in Fig. 3 is covered with a thin tin layer to avoid oxidization of the copper and to make connector soldering easier.

As discussed in Section 2.1, based on the orthogonal surface currents, the orthogonality of the modes can also be seen in Fig. 2(c) where simulated radiation patterns are presented at 2 GHz with Phi and Theta polarization components. The patterns correspond to the coordinate system in Fig. 2(a).

The simulated maximum realized gain is 4.1 dB for Port 1 and 1.3 dB for Port 2. The simulated total efficiency is 98% for Port 1 and 96% for Port 2. The total efficiency is the radiated power integrated over a sphere (P_r) related to the power delivered to the antenna port (P_{in}) [27]. In logarithmic scale, the total efficiency is calculated as $10 \cdot \log_{10}(P_r/P_{in})$. All the results are presented at 2 GHz center frequency.

2.3. Simulated and Measured *S*-Parameter Results

Figure 4 presents the measured and simulated S-parameters. The measured -10 dB impedance matching for S_{11} is from 1.87 GHz to 2.18 GHz, which limits the antenna operation band. On the other hand, the simulated results show 1.85–2.16 GHz bandwidth. As for S_{22}, both measured and simulated results

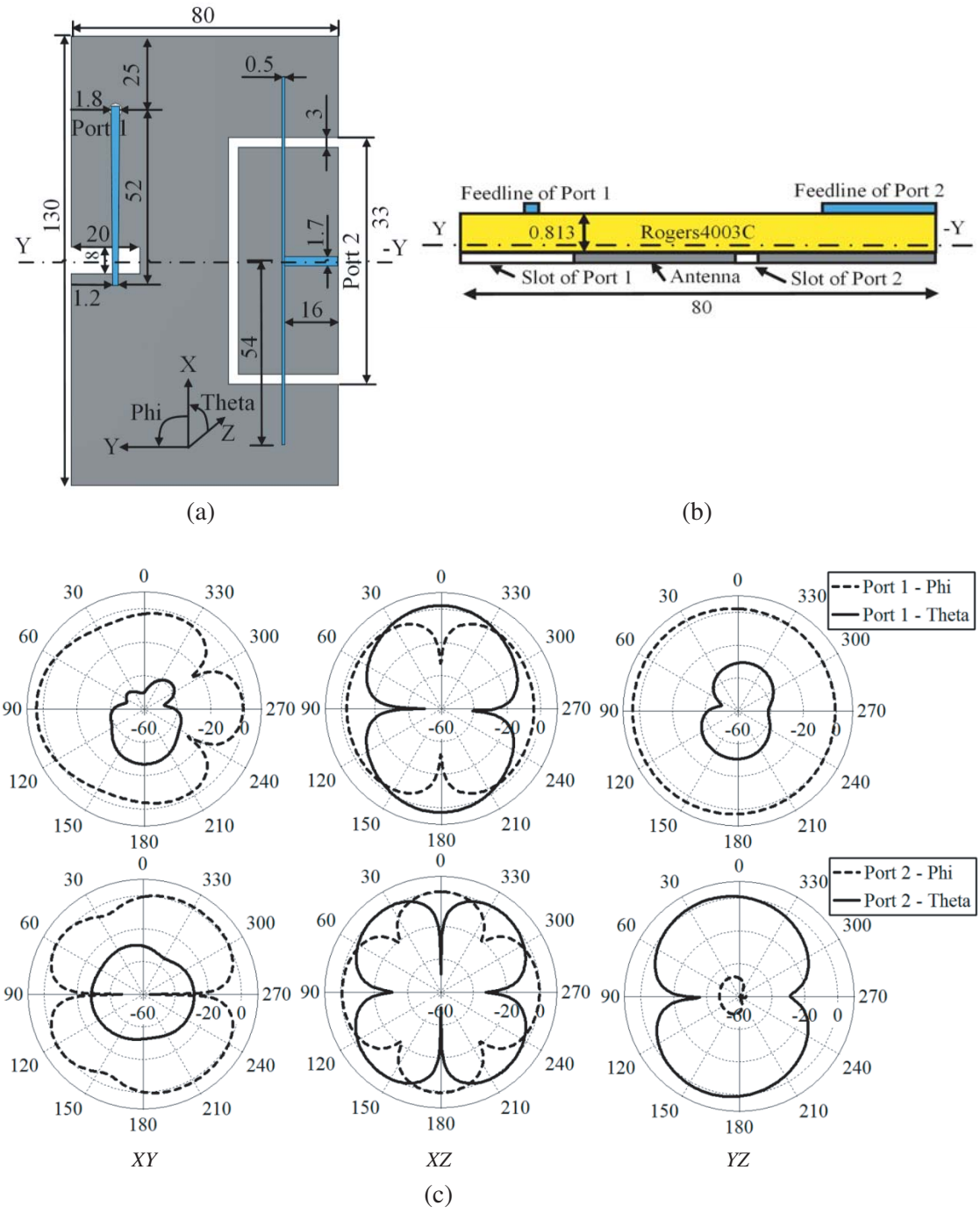

Figure 2. (a) Studied antenna structure with spherical coordinate system. (b) Up scaled antenna side view in Y-cut (line of dots and dashes). Antenna is drawn with gray color, feedlines with blue, and substrate in yellow. (c) Simulated radiation patterns with Phi and Theta polarization components of Port 1 (top row) and Port 2 (bottom row) at 2 GHz. Dimension in mm.

show below −10 dB matching. The difference between S_{11} and S_{22} comes from the different feeding network implementations. The simulated S_{21} predicts average −46.7 dB mutual coupling between the antenna ports, whereas the measured result shows −41.3 dB over the −10 dB impedance bandwidth. In general, it can be concluded that the simulated results predict the measured ones in a fair margin.

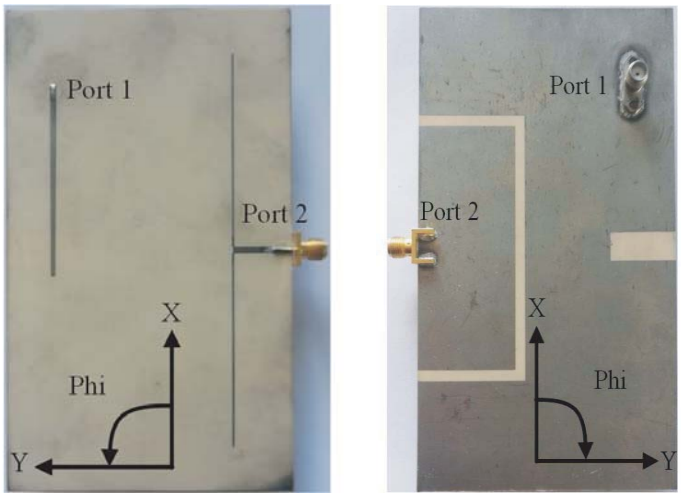

(a) (b)

Figure 3. Picture of prototype antenna on both sides with coordinate system.

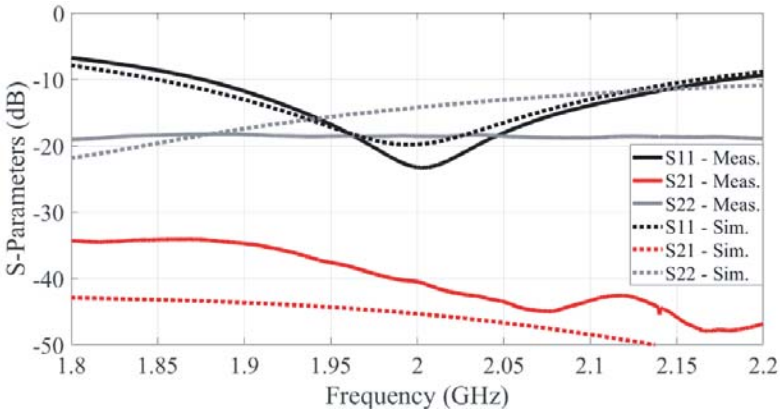

Figure 4. Simulated and measured S-parameters of the antenna structure.

3. 3GPP TRANSCEIVER FILTERING REQUIREMENTS

In this study, the antenna and RX intermodulation performances are tested with WCDMA TX power class 3, or 24 dBm level at Band 1 (2100 MHz band). The out-of-band (OOB) blocking requirement for WCDMA RX has been specified in [1]. The OOB requirement for a continuous wave interfering signal level in the antenna port is −15 dBm when the interfering signal is more than 85 MHz outside of the RX band.

The thermal noise level at WCDMA signal bandwidth is −108.1 dBm. The noise level at the antenna RX port, with specification assumed noise figure (NF) of 9 dB, is −99.1 dBm. The OOB testing generates IMD product, which falls on top of the RX signal. The maximum allowed IMD signal level is the same as noise level in the antenna port, which is −99.1 dBm.

The OOB testing is done conductively in standard based measurements, but in this study the OOB testing has been done Over-the-Air (OTA) manner to include filtering performance of the antenna to measurement results. The interfering blocker signal is WCDMA modulated to better emulate a real use-case scenario.

4. MEASUREMENT SETUP AND RESULTS

4.1. OTA Intermodulation Measurement Setup

The measurement setup is illustrated in Fig. 5, and a photograph of the actual measurement setup in an anechoic chamber is shown in Fig. 6. In Fig. 5, TX1 corresponds to PA1 (Power Amplifier 1) input, antenna Port 1 PA1 output, antenna Port 2 LNA (Low Noise Amplifier) input, and RX1 LNA output, respectively. TX2 is the power at PA2 (Power Amplifier 2) input, representing blocker signal before amplification. The distance between antennas ANT1 (Antenna 1) and ANT2 (Antenna 2) is 1 meter in the OTA measurements, and both have the same antenna structures (presented in Section 2, see Fig. 3). With ANT2 only Port 2 is used as it operates with the same mode as Port 2 of ANT1. Port 1 of ANT2 is terminated to 50 Ω load to avoid reflections.

Standard WCDMA uplink Band 1 signal at 1970 MHz was set to R&S (Rohde & Schwarz) SMIQ1 vector signal generator, and the signal was amplified with power amplifier PA1 (30 W LDMOS RF PA MRF21030) [28] and set to 24 dBm channel power at the node Port 1 of the ANT1. The receiver LNA

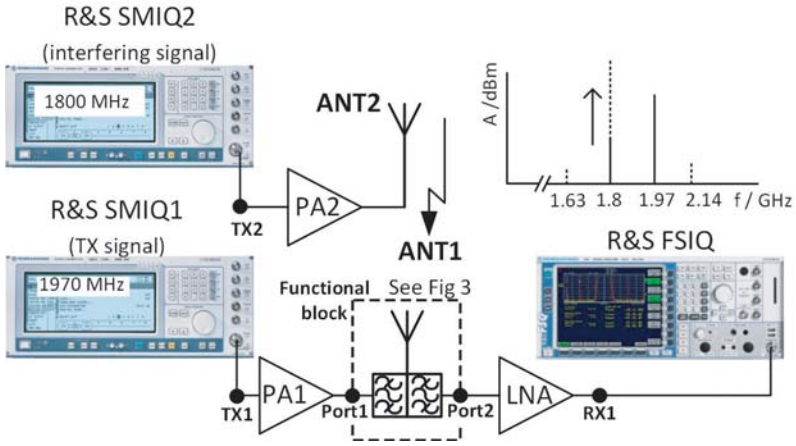

Figure 5. Illustration of the measurement test setup. ANT1 and ANT2 represent the antenna structure presented in Fig. 3. Spectrum above FSIQ presents the TX (1970 MHz), interference (1800 MHz), and measured RX1 (2140 MHz) signals in the test.

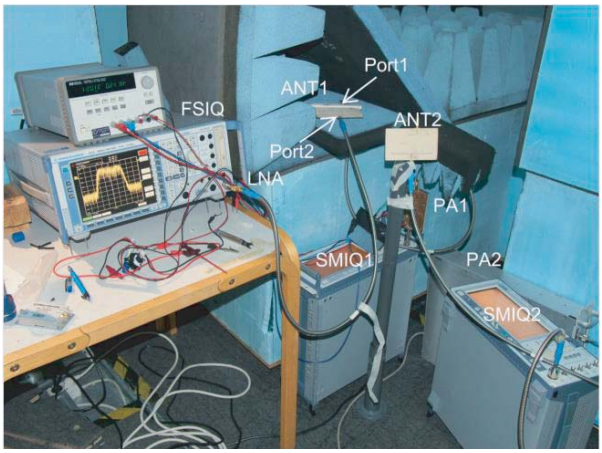

Figure 6. Measurement test setup in anechoic chamber. The setup is based on block diagram shown in Fig. 5.

used was Mini-Circuit ZLR-2400LN+, with the NF of 1.2 dB and the gain of 25.7 dB. The measured isolation between antenna ports, Port 1 and Port 2 of ANT1 at 1970 MHz, was measured to be 45 dB in OTA measurement. The result was slightly better than the measured value in Fig. 4, but also closer to the simulated value presented in Fig. 4. This was achieved by better minimizing the cable effect in the OTA measurements.

Interfering WCDMA uplink Band 3 signal (TX2) at 1800 MHz was generated with R&S SMIQ2 and amplified with PA2 (Ophir 5162 [29]), which provides 46 dB gain and maximum RF power of 28 W. This amplified blocker signal is then fed to ANT2. At the output of the LNA (RX1), the leaked TX1 signal and blocker signal are seen. In addition, nonlinearity of the LNA creates IMD product of these two WCDMA signals on the received channel at 2140 MHz.

The blocker signal power is swept and calibrated between 0 dBm and 20 dBm at the output of the LNA or RX1 node with R&S FSIQ, while the TX1 signal at 1970 MHz is kept constant 24 dBm. The calibration is counting out the antenna gains and free space loss. The channel power of the RX channel 2140 MHz caused by the high side of 3rd order intermodulation (IM3H) is measured in Port 2 and RX1 nodes to find the performance of the receiver with the use of the proposed highly isolated antenna structure without duplex filter. All the measurements equipment, including power amplifiers PA1 and PA2, operates on the linear region.

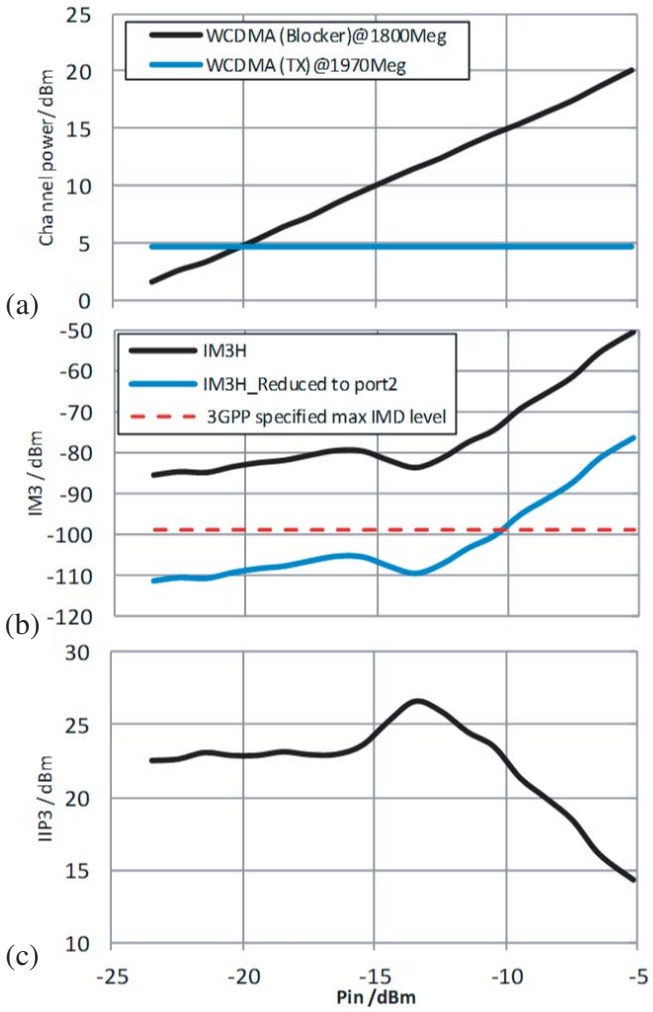

Figure 7. Measured channel power as a function of blocker signal at the input of the LNA (Port 2). (a) Input WCDMA signals at the output of the of the LNA (RX1 node), (b) measured channel power at 2140 MHz, i.e., IM3H and reduced IM3H to the input (Port 2), and (c) measured IIP3.

4.2. Measurement Results

The measurement results as a function of channel power of the blocker signal at the input of the LNA (Port 2) are shown in Fig. 7. The input signal of the LNA is swept by the blocker level from −23.5 dBm to −5.2 dBm. It can be seen in Fig. 7(a) that the channel power of the blocker signal at the RX1 node increases linearly from 0 dBm up to 20 dBm. At the same time, TX1 signal leakage remains constant 4.7 dBm (24 dBm − 45 dB + 25.7 dB).

The measured channel power of IM3H intermodulation at 2140 MHz is shown in Fig. 7(b), with the IM3H reduced to the input of the LNA (Port 2). It can be seen that the slope increases first 1 : 1 dB until there is an IMD sweet spot (i.e., IMD minimum) at $P_{in} = -13$ dBm. At higher input power levels, the IMD product increases with the slope of 4 : 1, meaning that the 5th and 7th order nonlinearities strongly affect IM3 (3rd Order Intermodulation). From the reduced IM3 curve, we can observe that IM3 is below the level of 3GPP specified −99.1 dBm limit almost up to −10 dBm of input power, which exceeds the standard requirement of −15 dBm. This is achieved by utilizing the proposed antenna structure with high antenna port isolation. Finally, the 3rd order input intercept point (IIP3) is shown in Fig. 7(c). It can be observed that the IIP3 level also remains above 22 dBm up to $P_{in} = -10$ dBm.

5. CONCLUSIONS

The paper presents an FDD study with a two-port antenna structure where both antenna ports were implemented to the same conducting body. The antenna has average 41.3 dB conductively measured isolation between the antenna ports over the studied −10 dB impedance bandwidth, which was 1.87 GHz to 2.18 GHz. The OTA measurement results showed that an antenna structure with highly isolated antenna ports fulfills the receiver intermodulation standard requirements without a duplex filter with maximum TX power level. The applications of the proposed structure with a high antenna port isolation can be found in mobile devices and small cell base stations.

ACKNOWLEDGMENT

This work was supported by Faculty of Information Technology and Electrical Engineering (ITEE), University of Oulu, in project "Frequency Division (and Full-) Duplex RF front-end demonstrator" (Fudut). The work was partially supported by the Academy of Finland 6Genesis Flagship (grant No. 318927).

REFERENCES

1. User equipment (UE) radio transmission and reception (Release 16) 3GPP TS 36.104 V16.1.0, Apr. 2019.
2. iPhone XR specification, available: https://www.apple.com/lae/iphone-xr/specs/.
3. Van Liempd, B., A. Visweswaran, S. Ariumi, S. Hitomi, P. Wambacq, and J. Craninckx, "Adaptive RF front-ends using electrical-balance duplexers and tuned SAW resonators," *IEEE Transactions on Microwave Theory and Techniques*, Vol. 65, No. 11, 4621–4628, Nov. 2017.
4. Sabharwal, A., P. Schniter, D. Guo, D. Bliss, S. Rangarajan, and R. Wich-Man, "In-band full-duplex wireless: Challenges and opportunities," *IEEE Journal on Selected Areas in Communications*, Vol. 32, 1637–1652, Sep. 2014.
5. Wang, X., W. Che, W. Yang, W. Feng, and L. Gu, "Self-interference cancellation antenna using auxiliary port reflection for full-duplex application," *IEEE Antennas and Wireless Propagation Letters*, Vol. 16, 2873–2876, Sep. 2017.
6. Douglas, T. J. and K. Sarabandi, "A high-isolation two-port planar antenna system for communication and radar applications," *IEEE Access*, Vol. 6, 9951–9959, Feb. 2018.
7. Zhou, C., H. Wong, and L. K. Yeung, "A wideband dual-polarized inductor-end slot antenna with stable beamwidth," *IEEE Antennas and Wireless Propagation Letters*, Vol. 17, No. 4, 608–612, Apr. 2018.

8. Ekrami, H. and S. Jam, "A compact triple-band dual-element MIMO antenna with high port-to-port isolation for wireless applications," *AEU — International Journal of Electronics and Communications*, Vol. 96, 219–227, Nov. 2018.
9. Gbafa, K., A. Diallo, P. Le Thuc, and R. Staraj, "Tx/Rx antenna system for full-duplex application," *IEEE International Symposium on Antennas and Propagation & USNC/URSI National Radio Science Meeting*, Boston, USA, Jul. 8–13, 2018.
10. Alsaif, H., M. Usman, M. T. Chughtai, and J. Nasir, "Cross polarized 2×2 UWB-MIMO antenna system for 5G wireless applications," *Progress In Electromagnetics Research M*, Vol. 76, 157–166, 2018.
11. Douglas, T. J. and K. Sarabandi, "Compact planar antenna system for full-duplex wireless applications," *IEEE International Symposium on Antennas and Propagation & USNC/URSI National Radio Science Meeting*, Boston, USA, Jul. 8–13, 2018.
12. Jaglan, N., S. D. Gupta, B. K. Kanaujia, S. Srivastava, and E. Thakur, "Triple band notched DG-CEBG structure based UWB MIMO/diversity antenna," *Progress In Electromagnetics Research C*, Vol. 80, 21–37, 2018.
13. Jiang, W., Y. Liu, Y. Cui, B. Wang, and S. Gong, "Compact wide-band MIMO antenna with high port isolation," *12th European Conference on Antennas and Propagation (EuCAP 2018)*, London, UK, Apr. 9–13, 2018.
14. Chaudhari, A. A. and R. K. Gupta, "A simple tri-band MIMO antenna using a single ground stub," *Progress In Electromagnetics Research C*, Vol. 86, 191–201, 2018.
15. Deo, P., D. Mirshekar-Syahkal, and G. Zheng, "EBG enhanced broadband dual antenna configuration for passive self-interference suppression in full-duplex communications," *15th European Radar Conference (EuRAD)*, Madrid, Spain, Sep. 26–28, 2018.
16. Zhai, H., L. Xi, Y. Zang, and L. Li, "A low-profile dual-polarized high-isolation MIMO antenna arrays for wideband base-station applications," *IEEE Transactions on Antennas and Propagation*, Vol. 66, No. 1, 191–202, Jan. 2018.
17. Marzouk, H. M., M. I. Ahmed, and A.-E. H. Shaalan, "Novel dual-band 28/38 GHz MIMO antennas for 5G mobile applications," *Progress In Electromagnetics Research C*, Vol. 93, 103–117, 2019.
18. Zhou, Z., Z. Wei, Z. Tang, and Y. Yin, "Design and analysis of a wideband multiple-microstrip dipole antenna with high isolation," *IEEE Antennas and Wireless Propagation Letters*, Vol. 18, No. 4, 722–726, Apr. 2019.
19. Nie, L. Y., X. Q. Lin, Z. Q. Yang, J. Zhang, and B. Wang, "Structure-shared planar UWB MIMO antenna with high isolation for mobile platform," *IEEE Transactions on Antennas and Propagation*, Vol. 67, No. 4, 2735–2738, Apr. 2019.
20. Feng, B., L. Li, J.-C. Cheng, and C.-T.-D. Sim, "A dual-band dual-polarized stacked microstrip antenna with high-isolation and band-notch characteristics for 5G microcell communications," *IEEE Transactions on Antennas and Propagation*, Vol. 67, No. 7, 4506–4516, Jul. 2019.
21. Yang, B., J. Zhou, and J. J. Adams, "A shape-first, feed-next design approach for compact planar MIMO antennas," *Progress In Electromagnetics Research M*, Vol. 77, 157–165, 2019.
22. Chen, Z., M. Li, G. Liu, Z. Wu, and M.-C. Tang, "Isolation enhancement for wideband, circularly/dual-polarized, high-density patch arrays using planar parasitic resonators," *IEEE Access*, Vol. 7, 112249–112257, Aug. 2019.
23. Zhang, P., S.-W. Qu, and S. Yang, "Dual-polarized planar phased array antenna with cavity-backed elements," *IEEE Antennas and Wireless Propagation Letters*, Vol. 18, No. 9, 1736–1740, Sep. 2019.
24. Li, Q., Y. Wei, M. Tan, X. Lei, G. Wu, M. Huang, and Y. Gong, "Flexibly extensible planar self-isolated wideband MIMO antenna for 5G communications," *MDPI Electronics*, Vol. 8, 994, Sep. 2019.
25. Aly, M. G., C. Mao, S. Gao, and Y. Wang, "A Ku-band filtering duplex antenna for satellite communications," *Progress In Electromagnetics Research M*, Vol. 85, 1–10, 2019.
26. Li, M., R. Wang, J. M. Yasir, and L. Jiang, "A miniaturized dual-band dual-polarized band-notched slot antenna array with high isolation for base station applications," *IEEE Transactions*

on Antennas and Propagation, (Early Access), Sep. 2019.

27. Milligan, T. A., *Modern Antenna Design*, 2nd Edition, 614, John Wiley & Sons, Inc., Hoboken, New Jersey, 2005.
28. NXP's MRF21030 LDMOS power transistor. Availbale: https://www.nxp.com/docs/en/data-sheet/MRF21030.pdf.
29. Ophir Solid state broadband high power RF amplifier. Available: https://ophirrf.com/wp-content/uploads/2015/10/5162.pdf.